Starlight beneath the waves : in search of TeV photon emission from Gamma-Ray Bursts with the ANTARES Neutrino Telescope

Laksmana-Astraatmadja, T.

11 Analysis of ANTARES data coinciding with two GRB events

In order to obtain an optimized quality cut for the selection of events, it is necessary to estimate first the number of expected signal. While analytical calculations such as performed in Chapters 2–3 can give this number, there are several limitations to it if we also want to include detector effects. The best way to estimate the number of signals that could be expected from a GRB with the given parameters is by performing a full Monte Carlo simulation from the top of the atmosphere to the bottom of the sea. A full treatment of Monte Carlo simulations allow us to include the effects due to muon multiplicity, the lateral distribution of the muons at sea level, and the stochastic effects of muon energy loss in water, and furthermore the effects of photon detection by the PMTs.

The discussion in this Chapter will be started with a description of the simulation chain employed for both target GRBs.

11.1 Muon production

Simulations of muon production from in the atmosphere are performed with `CORSIKA` (Heck et al., 1998) version 6990. Hadronic interactions in the atmosphere are simulated with the `QGSJET` model while the electromagnetic interactions are simulated with the `EGS4` package. The photon sources are fixed to the sky, with an azimuth and zenith distance conformed to the actual direction of the GRB.

The horizontal axes of `CORSIKA` are aligned with the Earth's north magnetic field, in order to include its effects to the tracks of the simulated particles. As noted by Guillard (2010), the effects of the Earth's magnetic field are negligible at TeV energy which is the interest of this study. Since there is negligible deviation due to magnetic field—which we shall also see later at reconstruction level—it is then safe to just consider that `CORSIKA` axes are aligned with the celestial North pole.

The results of the simulation are shown in Table 11.1 and Figure

No.	Name	α	δ	Azimuth	Altitude	N_γ	N_μ	$N_{s,\mathrm{HE}\mu}$
1	090709A	289.94	60.73	331.62	25.09	$\sim 10^8$	11 706 524	24765
2	070220	34.80	68.80	4.68	22.05	$\sim 5 \times 10^7$	4 179 214	10638

Table 11.1: Summary of the CORSIKA simulation. All positional coordinates are in degrees. Azimuth is measured from the celestial North and is positive toward the East. Altitude is measured from the local horizon, positive towards the zenith and negative towards the nadir. N_γ is the total number of generated photons and N_μ is the total number of muons generated in the atmosphere. $N_{s,\mathrm{HE}\mu}$ is the number of muon showers containing at least one muon with energy higher than 500 GeV. The photon and muon spectra are shown in Figure 11.1.

11.1. The spectrum is calculated using an analytical formulation involving the attenuation of TeV photons by the cosmic infrared background (CIB). Because attenuation is involved, the shape of the photon is then no longer in the form of a simple power sample, i.e. $dN_\gamma/d\epsilon_\gamma \propto \epsilon_\gamma^{-\beta}$, where β is the spectral index of the photon spectrum's high-enery component. Instead, the shape of the photon spectrum will be in the form of

$$\frac{dN_\gamma}{d\epsilon_\gamma} \propto \epsilon_\gamma^{-\beta} e^{-\tau_{\gamma\gamma}(\epsilon_\gamma, z)}, \tag{11.1}$$

where $\tau_{\gamma\gamma}(\epsilon_\gamma, z)$ is the optical depth of the universe along the line of sight to the GRB, as a function of the photon energy in the observer frame ϵ_γ and the redshift z of the GRB. The optical depth $\tau_{\gamma\gamma}$ increases with increasing photon energy and redshift. Attenuation then get more severe. This is discussed in more detail in Section 2.3.

Because CORSIKA can only generate photons according to simple power law, a certain trick has to be used so that it will generate photons from an attenuated spectrum. The trick invented for this purpose is to chop the attenuated spectrum into small bins and calculate the number of photons that should be generated in the bin. This is done first by normalizing the spectrum to the total number of photons N_γ we want to generate:

$$N_\gamma = f_\gamma \int_{\epsilon_{\gamma,\mathrm{min}}}^{\epsilon_{\gamma,\mathrm{max}}} d\epsilon_\gamma \epsilon_\gamma^{-\beta} e^{-\tau_{\gamma\gamma}(\epsilon_\gamma, z)}. \tag{11.2}$$

From this equation it is straightforward to calculate the normalization factor f_γ. The minimum energy $\epsilon_{\gamma,\mathrm{min}}$ is set to 1 TeV and the maximum energy $\epsilon_{\gamma,\mathrm{max}}$ is arbitrarily set to 300 TeV. We could then chop the spectrum into a number of n bins of equal bin width:

$$\Delta \log \epsilon_\gamma = \frac{1}{n} \log \left(\frac{\epsilon_{\gamma,\mathrm{max}}}{\epsilon_{\gamma,\mathrm{min}}} \right), \tag{11.3}$$

and calculate the number of photons that should be generated

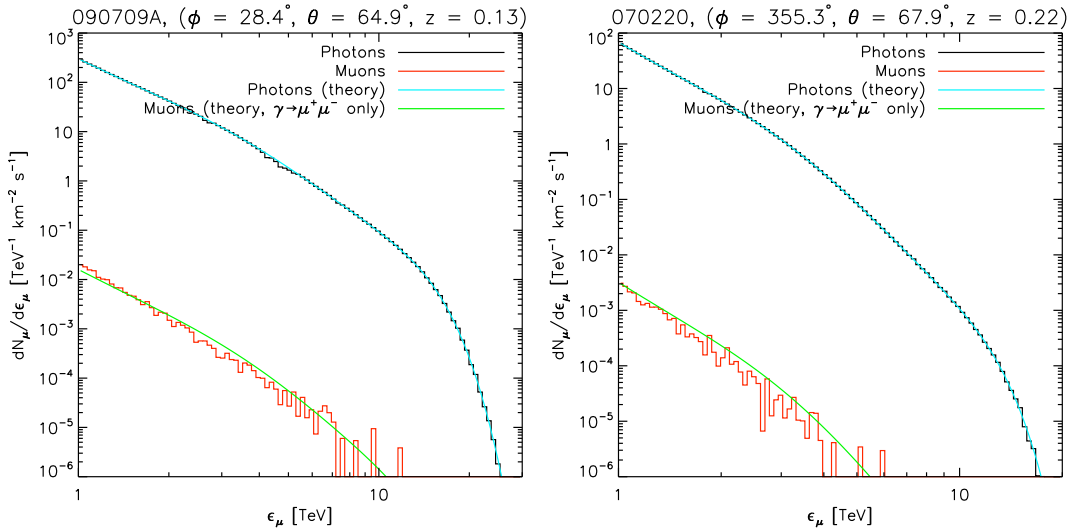

Figure 11.1: The shape of the photon spectrum used to generate photons, and the resulting muon spectrum. The solid line on top of the photon histogram is the theoretical photon spectrum, while the solid line on top of the muon histogram is the theoretical calculation of the muon spectrum.

within the i-th bin:

$$N_{\gamma,i} = f_\gamma \epsilon_{\gamma,i} \ln(10) \Delta \log \epsilon_\gamma \frac{dN_\gamma}{d\epsilon_{\gamma,i}} e^{-\tau_{\gamma\gamma}(\epsilon_{\gamma,i}, z)}. \tag{11.4}$$

The number of muons inside each bins as well as the minimum and maximum energy is then used as input to `CORSIKA` along with other required input. The resulting spectrum could then mimic the attenuated spectrum, as we can see in Figure 11.1.

Using this method, the calculation of the weights of the simulated events reduces to a single constant value and is invariable to energy.

11.2 *Muon duplication*

The column with header $N_{s,\mathrm{HE}\mu}$ in Table 11.1 shows the number of muon showers that contain at least one muon with energy higher than 500 GeV. The content of the muon bundle generated in one photon shower can go up to hundreds of muons, although within this bundle of muons normally there would only be one or two very high energy muons. The number of showers containing high-energy muons are too low if we also think that they have to be propagated to the detector and then reconstructed, but increasing the number of photons to be simulated will increase the

amount of computer time. It is faster to duplicate these showers and treat them as if they are different events.

It is also necessary to not only duplicate the muons but also to spread them into a more extended beam that covers all part of the detector. The generating area of the photons within CORSIKA is concentrated only to a beam with radius ∼20 m, which is too small compared to the size of the detector which radius is ten times the corsika beam radius. If we only propagate photons from a pencil beam, we would only simulate a small part of the detector which may introduce a bias in the result of the simulation.

The definition of the photon duplicating area at the surface must not be too large that muons at its edge would never be detected and thus waste computer time, but also must be large enough that it efficiently covers all part of the detector. One scheme that meets these requirements is shown in Figure 11.2. This scheme requires the dimension of the can that covers the instrumented volume, the vertical location of the detector's centre of gravity, the depth of the sea, and the direction of the GRB in local coordinates azimuth ϕ and zenith distance θ.

The basic idea is as follows: First we draw a circumscribing sphere around the can. It is straightforward to calculate the radius r_s of this sphere (Figure 11.3):

$$r_s = (\tfrac{1}{4}h_c^2 + r_s^2)^{1/2}, \tag{11.5}$$

where h_c is the height of the can which can be obtained if we know the vertical coordinates of the top and bottom and surface of the can:

$$h_c = z_{c,\max} - z_{c,\min}. \tag{11.6}$$

We can then draw a tube with radius r_s that points to the direction (ϕ, θ) of the GRB. This tube represents the beam of photon-induced muons. The muons inside this beam will hit all parts of the detector because the beam exactly covers the can. The cylindrical section of the tube that parallels the plane of the sea surface is then simply the muon duplication area, and is in the shape of an ellipse with semimajor axis

$$a = \frac{r_s}{\cos\theta}, \tag{11.7}$$

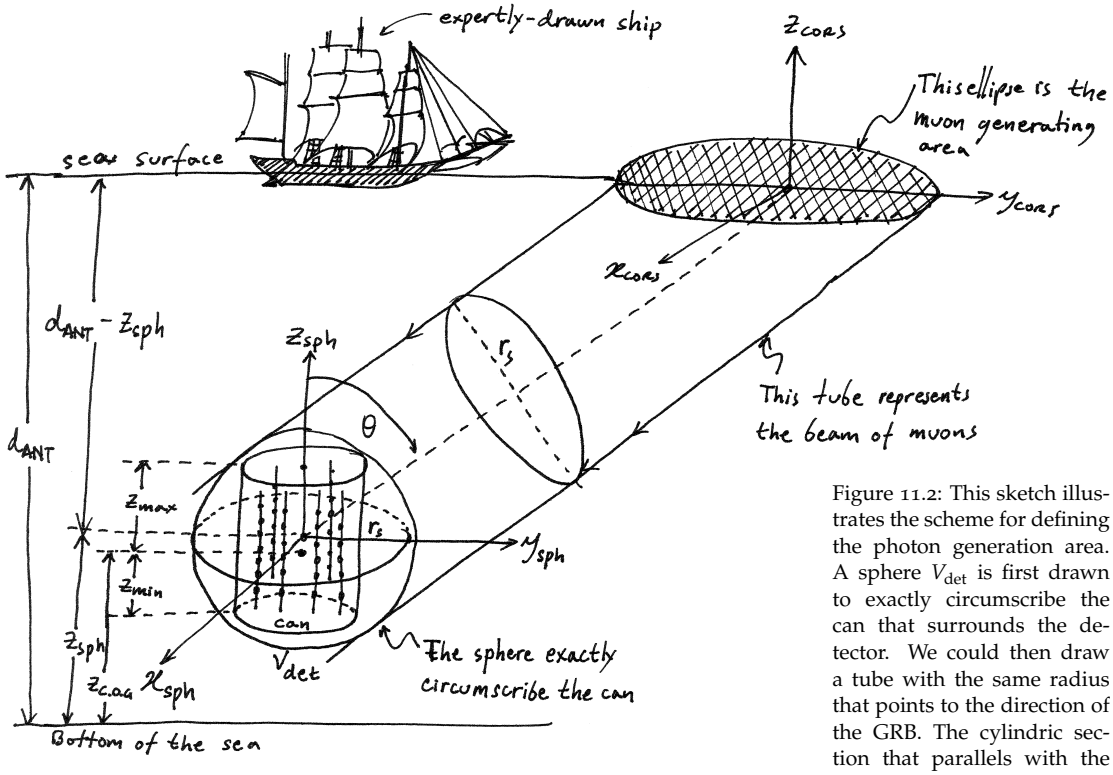

Figure 11.2: This sketch illustrates the scheme for defining the photon generation area. A sphere V_{det} is first drawn to exactly circumscribe the can that surrounds the detector. We could then draw a tube with the same radius that points to the direction of the GRB. The cylindric section that parallels with the plane of the sea surface is then the photon generation area, which will be an ellipse. Illustration by the author.

and semiminor axis is $b = r_s$. Because the tube points to the direction of the GRB, the axes of the ellipse is inclined with angle ϕ relative to the axes of the coordinate system. The area of the ellipse is $A_{\text{ellipse}} = \pi ab$.

The coordinates of the center of the ellipse relative to the center of gravity of the detector can be obtained if we know the depth of the sea d_{ANT} and the vertical coordinates of the detector's center of gravity $z_{\text{C.O.G}}$. The coordinates for the center of gravity of the detector can be obtained from the `km3` program. The vertical distance d_s of the circumscribing sphere to the surface is then

$$z_s = z_{\text{C.O.G}} + z_{c,\text{max}} - \tfrac{1}{2}h_c, \tag{11.8}$$

$$d_s = d_{\text{ANT}} - z_s. \tag{11.9}$$

Here z_s the vertical coordinates of the circumscribing sphere. The

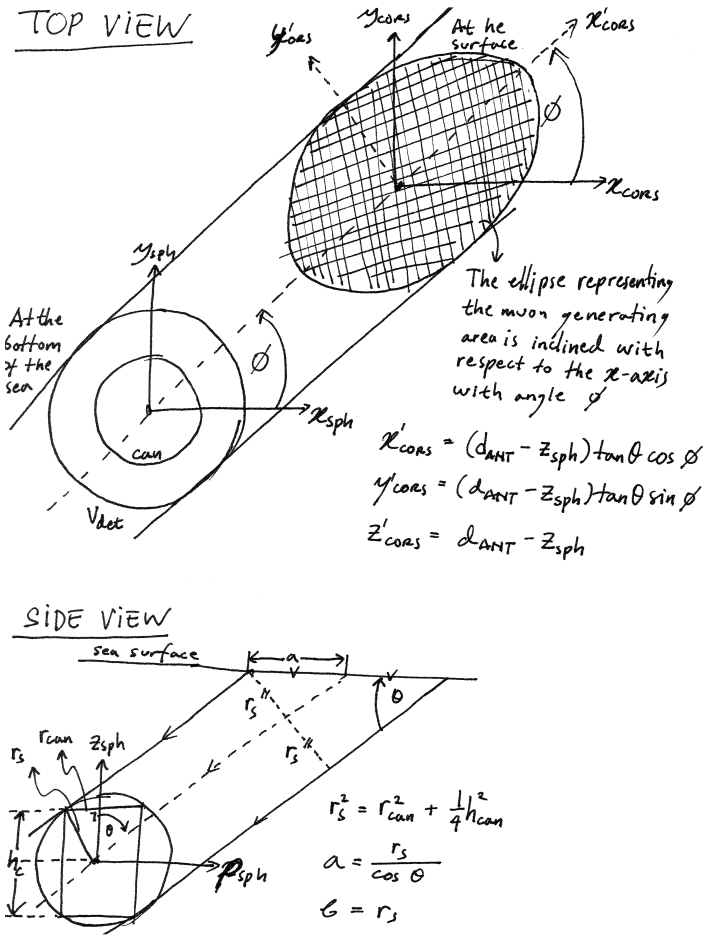

Figure 11.3: The top-view and side-view of the muon generating area and its orientation with respect to the can. Because the tube representing the beam of TeV photon-induced muons are directed toward the source, the ellipse representing the muon generating area is inclined with angle $\phi = 360^\circ - \text{Azimuth}$ with respect to the x-axis. Calculating the size of the ellipse with respect to the can is straightforward if we consider a sphere exactly circumscribing the can. Illustration by the author.

coordinates of the center of the ellipse is then

$$\mathbf{r}_{\text{ellipse}} = \begin{bmatrix} x_{\text{ellipse}} \\ y_{\text{ellipse}} \\ z_{\text{ellipse}} \end{bmatrix} = \begin{bmatrix} d_s \tan\theta \cos\phi \\ d_s \tan\theta \sin\phi \\ d_s \end{bmatrix} \tag{11.10}$$

We could now generate random points within this ellipse that would be the new coordinates of the muons relative to the center of gravity of the detector. First we generate two random numbers $\{R_1, R_2\} \in [0, 1]$. Using these two random numbers we could then calculate the coordinates at the sea surface relative to the center of

No.	Name	ϕ	θ	$N_{s,\mathrm{HE}\mu}$	Duplication	Run No.	N_{rec}	μ_s
1	090709A	28.38	64.91	24 765	50 000	41812	27 221	2.7×10^{-4}
2	070220	355.32	67.95	10 638	1 200 000	26128	912	6.5×10^{-8}

Table 11.2: Summary of the detector simulation. All positional coordinates are in degrees. ϕ is measured from the celestial North and is positive toward the West, thus $\phi = 360^\circ -$ Azimuth. θ is measured from the zenith and is positive toward the nadir, and $\theta = 90^\circ -$ Altitude. $N_{s,\mathrm{HE}\mu}$ is the number of photons that generate muon showers containing at least one muon with energy higher than 500 GeV. Duplication is the number of times $N_{s,\mathrm{HE}\mu}$ are duplicated. Run No. is the raw data file used for background simulation, N_{rec} is the final number of events at reconstruction level. μ_s is the number of weighted signal events.

the ellipse $\mathbf{r}_{\mathrm{ellipse}}$:

$$\mathbf{r}'_{\mathrm{surf}} = \begin{bmatrix} x'_{\mathrm{surf}} \\ y'_{\mathrm{surf}} \end{bmatrix} = \begin{bmatrix} -a + 2aR_1 \\ -b + 2bR_2 \end{bmatrix} \tag{11.11}$$

This generated coordinates will be accepted if the criterion

$$\left(\frac{x'_{\mathrm{surf}}}{a}\right)^2 + \left(\frac{y'_{\mathrm{surf}}}{b}\right)^2 < 1 \tag{11.12}$$

is satisfied. Next we rotate the coordinates by an angle ϕ:

$$\mathbf{r}_{\mathrm{surf}} = \begin{bmatrix} x_{\mathrm{surf}} \\ y_{\mathrm{surf}} \end{bmatrix} = \begin{bmatrix} \cos\phi & -\sin\phi \\ \sin\phi & \cos\phi \end{bmatrix} \begin{bmatrix} x'_{\mathrm{surf}} \\ y'_{\mathrm{surf}} \end{bmatrix} \tag{11.13}$$

The new coordinates for the muon will then be

$$\mathbf{r}_\mu = \mathbf{r}_{\mathrm{ellipse}} + \mathbf{r}_{\mathrm{surf}} + \mathbf{r}_{\mu,0}, \tag{11.14}$$

where $\mathbf{r}_{\mu,0}$ are the original 2D coordinates of the muon at the sea surface, obtained from `CORSIKA` simulation. It is worthwhile to note here that $\mathbf{r}_\mu$ are 3D coordinates with the same vertical components, i.e. $z_{\mathrm{ellipse}} = d_s$.

This algorithm is repeated for all muons. The muons are also duplicated to increase the statistics at reconstruction level. The number of duplications are shown in Table 11.2.

The final position of the muons is shown in Figure 11.4. We can see that our calculations are correct since the size and orientation of the ellipse are correct and that the muons do point toward the detector.

11.3 *Further simulation chains*

MUON propagation from the sea surface towards the can is performed using the `MUSIC` code (Antonioli et al., 1997) that runs within the `km3` software. Furthermore, `km3` is also used to generate the Cherenkov photons and hits detected by the PMTs. The response of ANTARES to the photons is then simulated with `TriggerEfficiency`, and the tracks are reconstructed with the `aafit v0r9` algorithm.

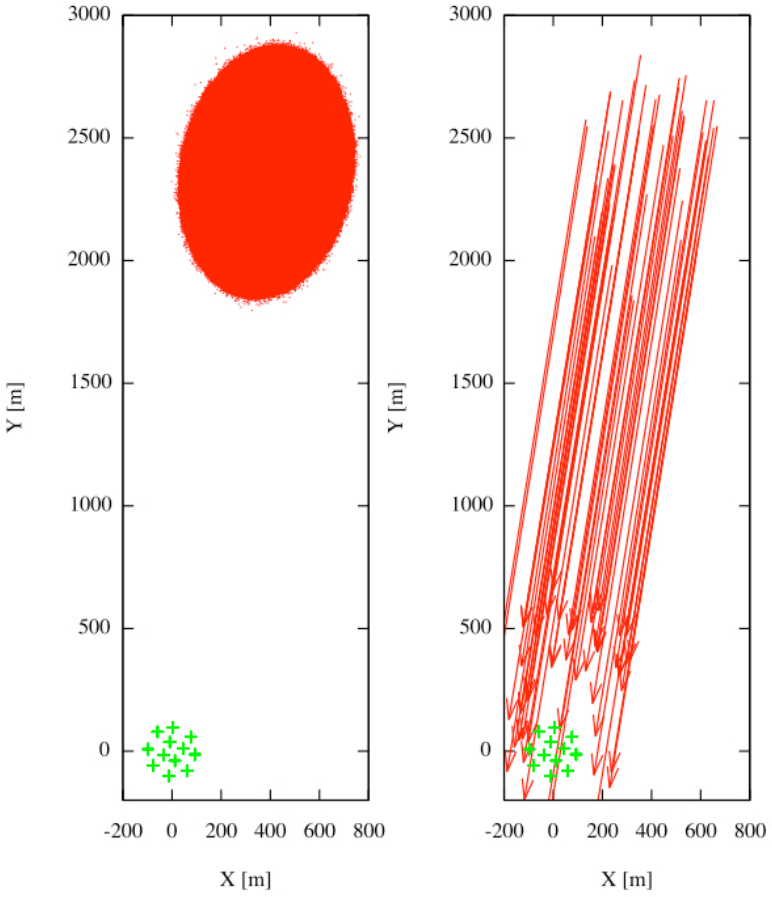

Figure 11.4: The initial positions (left) and momentum vectors (right) of the muons at the surface, relative to the center of gravity of the detector. The red dots in the left plot shows the final coordinates of the initial positions of the muons, after coordinate rotation has been performed. Green crosses show the positions of the detector strings. As we can see, the muons are distributed inside an ellipse with the prescribed size, as well as the inclination relative to the X-axis. In the right plot, the momentum vectors of several muons are shown, to make sure that they do point toward the detector.

To emulate environmental and detector conditions, the random background hits in `TriggerEfficiency` are generated by using input parameters obtained from the raw data file corresponding to the time when the GRBs took place. The quality of the data taken during the corresponding the run is shown Table 11.3.

11.4 *Results of the reconstruction*

The final number of events at reconstruction level is shown in Table 11.2. This is the total number which already includes duplication. The expected number of signal μ_s is shown in the last

Run No.	41812	26128
Baseline rate [kHz]	67.76	
Burst fraction	0.43	
Expected muon [minute^{-1}]	83.18	
Number of active lines	9	
Theoretical number of OMs	645	375
Number of active OMs	486	
Mean active OMs	509.91	
Mean rate [kHz]	96.45	118.91
Median trigger hits	12.19	
Number of muons [minute^{-1}]	84.90	
Data quality	1	
Run duration [s]	15704	

Table 11.3: Data quality of the runs containing the selected GRBs. These values are taken from the ANTARES database.

column, where

$$\mu_s = w_s N_{\text{rec}}, \tag{11.15}$$

here w_s is the weight of each individual signal event. Because of the way we generate the photons, the shape of the generated photon spectrum reproduces the expected photon spectrum. Consequently, the weight of each individual signal event w_s is invariant to the energy ϵ_γ of the photons, and the value is the same for all signal events:

$$w_s = \frac{\frac{dN_\gamma}{d\epsilon_\gamma}\Big|^{\text{th}}_{\epsilon_\gamma}}{\frac{dN_\gamma}{d\epsilon_\gamma}\Big|^{C}_{\epsilon_\gamma}} \frac{T_{90} A_{\text{ellipse}}}{N_{\text{duplication}}}. \tag{11.16}$$

Here $\frac{dN_\gamma}{d\epsilon_\gamma}\Big|^{\text{th}}_{\epsilon_\gamma}$ is the theoretical photon spectrum at a certain energy ϵ_γ, $\frac{dN_\gamma}{d\epsilon_\gamma}\Big|^{C}_{\epsilon_\gamma}$ is the `CORSIKA` photon spectrum at the same photon energy, T_{90} is the burst duration, A_{ellipse} is the size of the ellipse generating area, and $N_{\text{duplication}}$ is the number of muon duplication performed.

11.4.1 Detection efficiency

THE PLOTS that describe the detection efficiency η_μ for each GRB is shown in Figure 11.5. For each GRB, the muon spectrum at

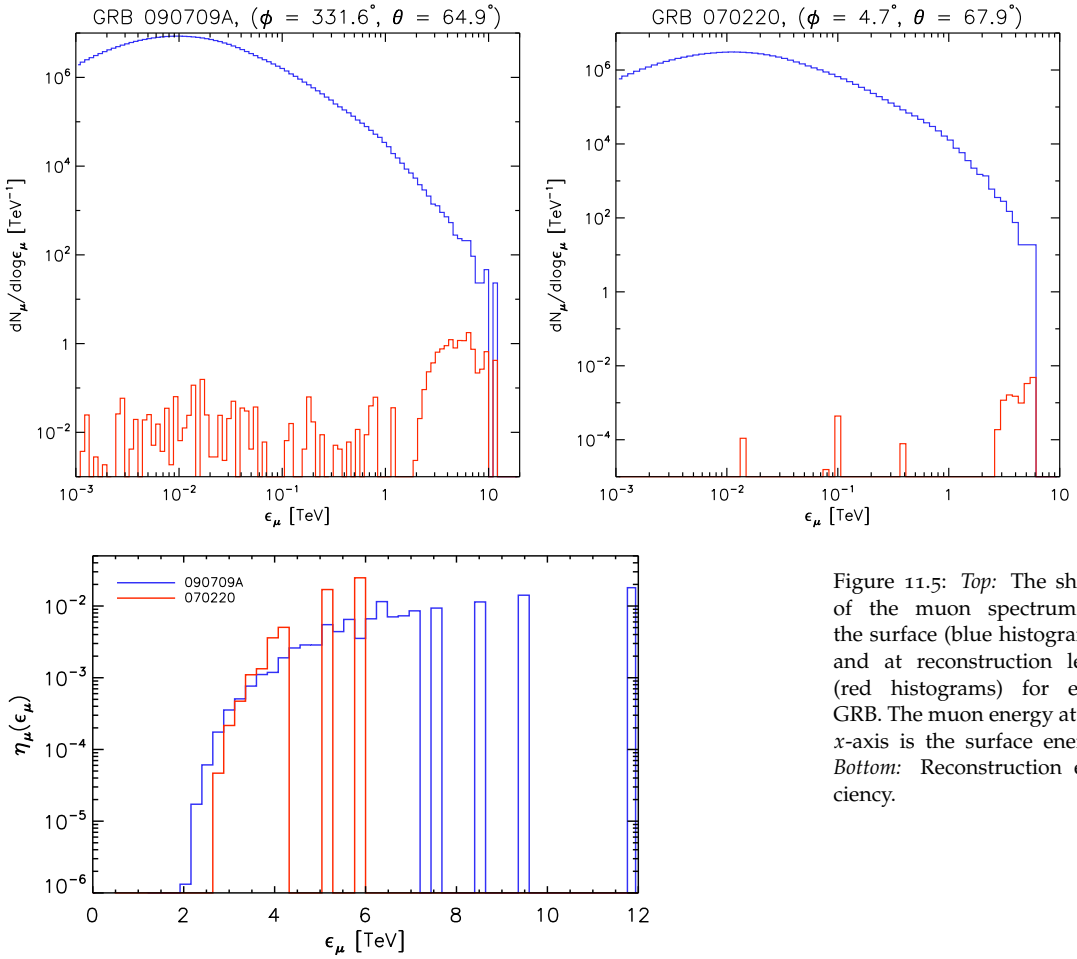

Figure 11.5: *Top:* The shape of the muon spectrum at the surface (blue histograms) and at reconstruction level (red histograms) for each GRB. The muon energy at the x-axis is the surface energy. *Bottom:* Reconstruction efficiency.

the sea surface is shown as the blue histogram, while the muon spectrum at reconstruction level is shown as the red histogram. The muon energy used at the x-axis is the muon energy at the sea surface. We can see that low-energy muons could penetrate the depth of the sea and be reconstructed, albeit with low efficiency. High-energy muons with $\epsilon_\mu \geq 1$ TeV still comprise the majority of the reconstructed tracks. At the bottom plot of Figure 11.5, the detection efficiency η_μ as a function of the muon energy is plotted for each GRB.

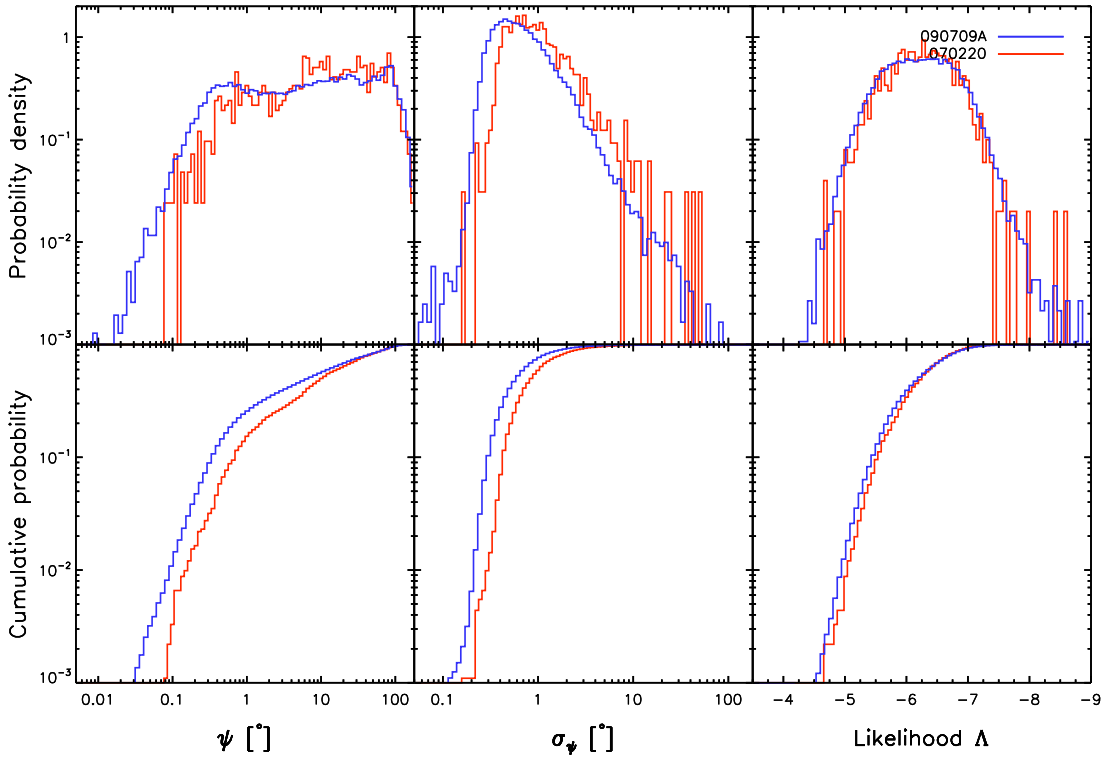

Figure 11.6: The probability distribution function (PDF) and cumulative distribution function (CDF) of the true angular resolution ψ (left), the angular uncertainty σ_ψ (center), and the fit likelihood Λ (right). Different color indicates different GRB, as indicated in the legend.

11.4.2 *Track reconstruction quality*

The distribution of the relevant parameters that define the quality of the reconstruction are shown in Figure 11.6. This Figure shows the distribution of the true angular resolution ψ, angular error estimate σ_ψ, and the goodness-of-fit Λ for both GRBs.

We can see that the distribution of σ_ψ and Λ is consistent with previous simulations shown in Chapter 7. The distribution of ψ however is different with what we would expect from a source at this zenith distance. This could arise from the fact that we are simulating the detector with realistic conditions, and that the detector conditions at the time the GRB took place was below the idealized optimum conditions. Table 11.3 shows the quality of the data taken in the run when the selected GRB events happened, as well as the detector condition at that moment. We can see that

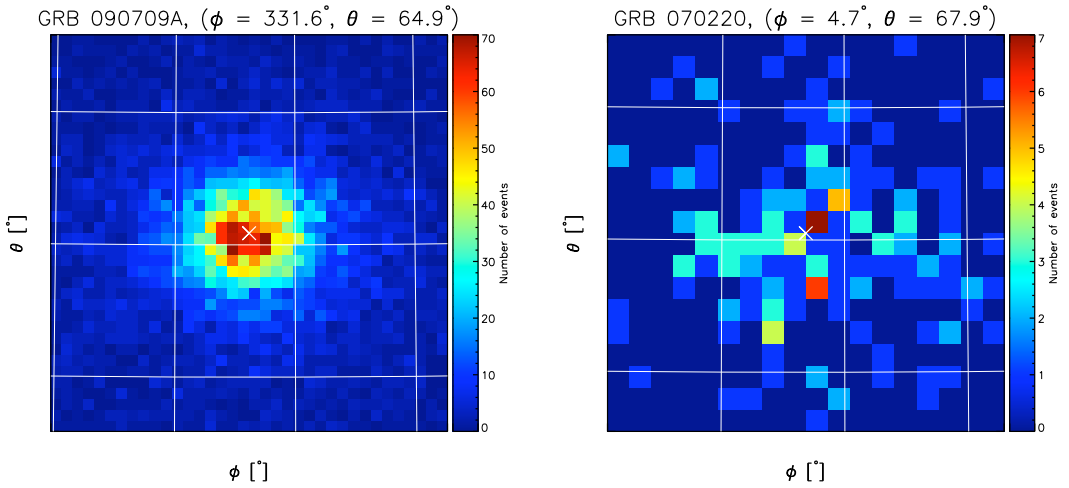

Figure 11.7: The point spread function (PSF) of the muon events of the GRBs, drawn in Lambert azimuthal equal-area projection. The size of the box is $3^\circ \times 3^\circ$ and the width between grid lines is 1°. The plot is centered on the supposed location of the GRB, marked by the white cross in the middle of each plot. For illustration purpose, the weight for each events is set to 1.

when GRB 090709A (run number 41812) went off, only 9 lines out of the total 12 were active at that time. GRB 070220 (run number 26128) happened when the ANTARES detector consisted of only 5 lines. The quality of the data taken were category 1 for run number 41812. Quality 1 indicate that the data taken surpass the basic quality criteria and are suitable for physics analysis.

The point spread function of the reconstructed events for each GRB is shown in Figure 11.7. Here the weight of events are set to $w_s = 1$ for illustration purpose. We can see that most of the interesting signal events are well-reconstructed, within a radius of the PSF is $\sim 1^\circ$.

11.5 *Optimization*

The optimization results for the model discovery potential (MDP) approach are shown in Figures 11.8–11.9 and Table 11.4, while the

GRB	MDP (3σ)		MDP (5σ)		MRF	
	Ψ [°]	Λ_{aafit}	Ψ [°]	Λ_{aafit}	Ψ [°]	Λ_{aafit}
090709A	1.43	-6.29	1.24	-6.25	2.82	-6.55
070220	1.04	-6.12	7.29	-6.92	9.68	-7.00

Table 11.4: The combination of cuts for each GRB that minimizes the MDP and MRF.

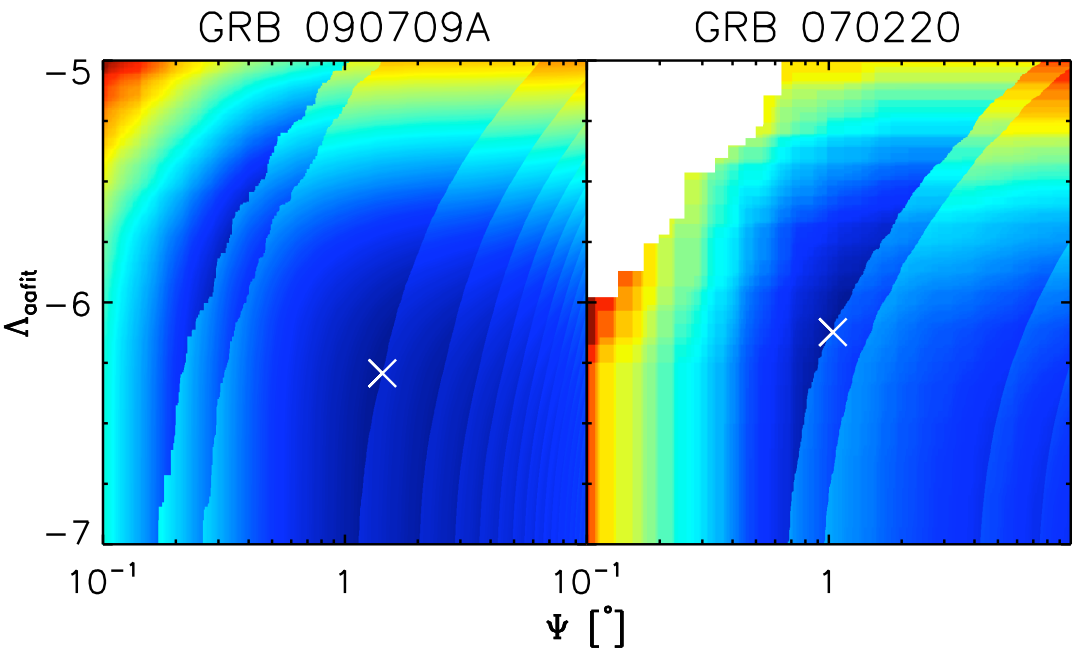

Figure 11.8: The model discovery potential (MDP) for a 50% probability of making a 3σ discovery, as a function of opening radius Ψ and Λ, for both GRBs. The cut in Ψ and Λ that minimizes the MDP is shown as the white cross in the plot.

results for the model rejection factor (MRF) is shown in Figure 11.10 and Table 11.4. The optimization result is reasonable given that the expected number of signal events are very low.

11.5.1 Expected significance of the observation

We could calculate the significance of the detection using the significance formula derived by Li & Ma (1983), which is based on the likelihood ratio method. For this calculation, an "ON" and "OFF" period must be defined: The "ON" time is the period in which we know there is a GRB event, while "OFF" is the period in which we know there is only background. For simplicity of the calculation we could define $t_{\rm on}$ as the T_{90} of the GRB, and $t_{\rm off}$ as the one hour period before the GRB in question took place. We

No.	Name	$t_{\rm on}$	$t_{\rm off}$	$n_{\rm on}$	$n_{\rm off}$	S
1	090709A	344.85	3600	0.07	0.76	2.52×10^{-4}
3	070220	150.67	3600	0.32	7.60	3.03×10^{-8}

Table 11.5: Summary of the Li & Ma (1983) significance calculation. On-time $t_{\rm on}$ and off-time $t_{\rm off}$ are in seconds. $n_{\rm on}$ and $n_{\rm off}$ are the expected number of events during the respectively on and off period. The significance of the detection S is shown in the last column.

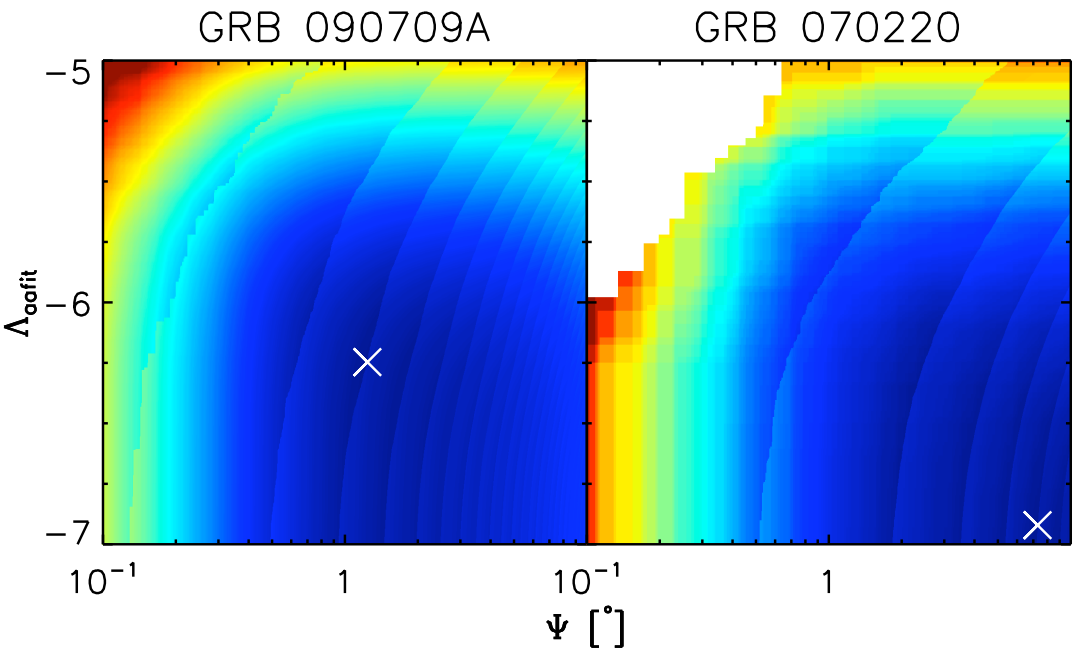

Figure 11.9: The same as in Figure 11.8, but for a 50% probability of making a 5σ discovery.

measure the number of events during the "ON" period, n_{on}, as well as the number of events during the "OFF" period, n_{off}. From these four quantities, we can measure the significance S of the detection.

The results of these calculations are shown in Table 11.5. The expected significances for all GRBs are very low, despite the very low background rate. This is because the expected number of signal events itself is very low. Unless there is an enhancement of signal events at the source itself, this is the significance we could expect after unblinding of the data.

As the number of background events are very low, the observation time during the "off" period is taken to be 60 minutes.

11.5.2 Expected sensitivity

The expected sensitivity plot for each individual GRBs is shown in Figure 11.11. This expected sensitivity is calculated by multiplying the theoretical photon spectrum by the value of the mini-

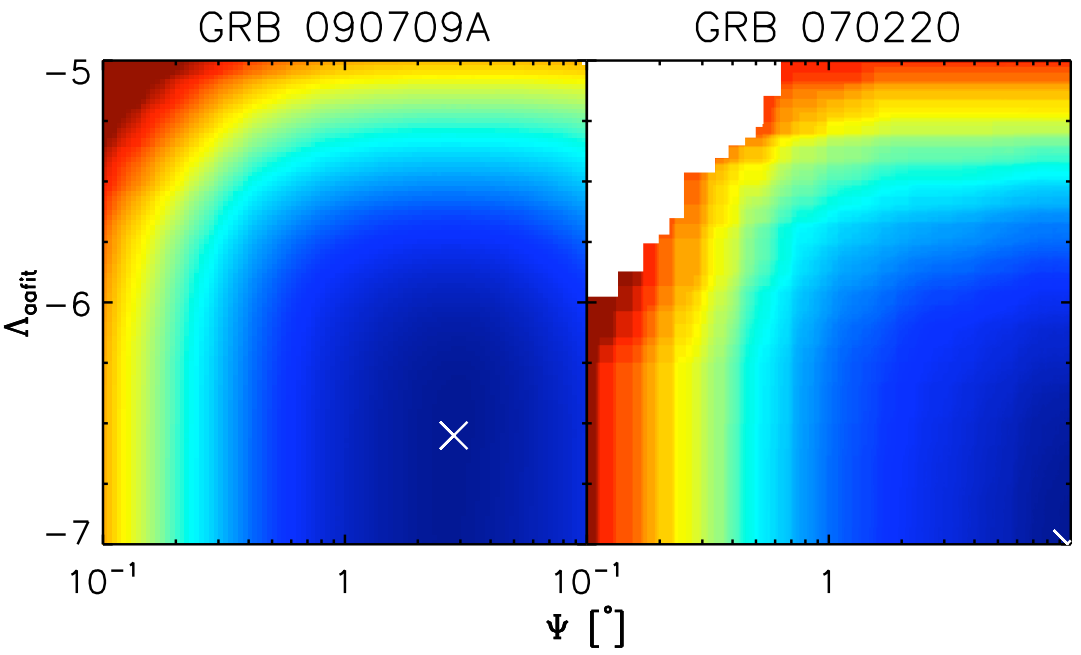

Figure 11.10: The plots for the 90% confidence limit model rejection factor (MRF), as a function of opening radius Ψ and Λ, for the each proposed GRBs. The set of cuts that minimized the MDP and the MRF is shown as the white X in the each plot.

mum MRF:

$$\phi_{90}(\epsilon_\gamma) = \frac{\bar{\mu}_{90}(\mu_b)}{\mu_s}\phi(\epsilon_\gamma), \tag{11.17}$$

where μ_s and μ_b are respectively the expected values of the signal and background that pass the quality cuts that minimize the MRF, and $\bar{\mu}_{90}(\mu_b)$ is the averaged upper limit at 90% confidence level. After the unblinding, this sensitivity will be recalculated by inserting the measured background and signal.

As we can see, ANTARES sensitivity is low for a GRB with a small flux. Unless there is an enhancement of TeV photon production at the source itself, we would not expect to see any event. However, since we are observing the GRB event from start to finish, this would be a very compelling limit in the TeV regime.

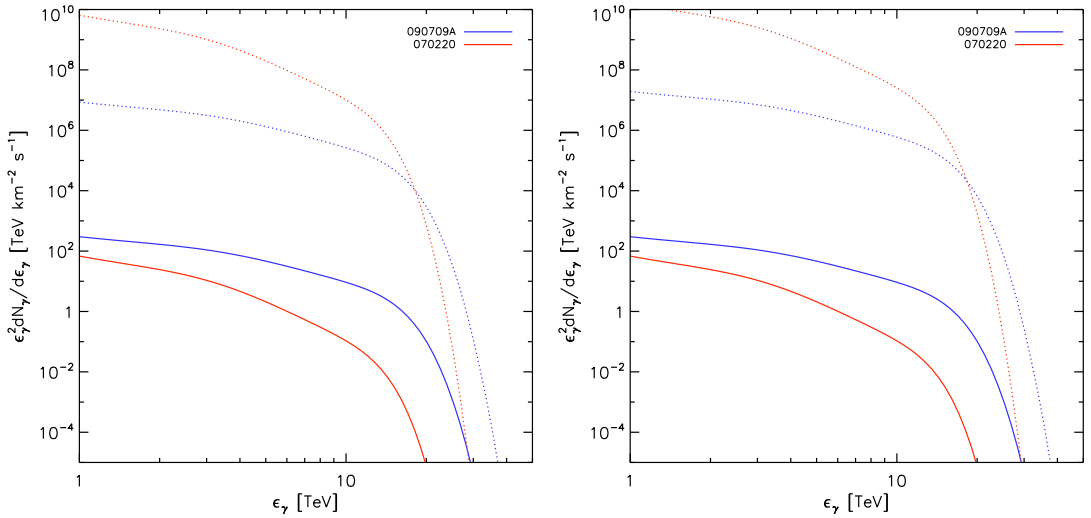

Figure 11.11: The expected sensitivity of ANTARES to each GRBs, shown here in dotted lines. The theoretical photon spectrum is shown in solid lines. The left plot shows the sensitivity if the MRF result approach is used, while the right plot shows the sensitivity if the MDP 5σ approach is used. If the MDP values are used, the detector is slightly less sensitive than if the MRF results are used.

11.6 Summary

The individual optimization of the top two GRBs proposed to be unblinded has been performed. Using `CORSIKA` to simulate muon production in the atmosphere, the spatial distribution of high-energy muons at the surface has been obtained and has been put into good use.

A set of cuts that minimized the MDP and MRF has been obtained, and the expected detection significance and limit of the observation has been calculated. In principle all the necessary analysis for unblinding has been performed.

Due to the very low expectation to observe any signal event from GRB 070220 because of the small instrumented volume of the detector when the GRB happened, it was proposed that this GRB is dropped from the observation proposal. We will observe then only one GRB instead of two.

In summary, further analysis after unblinding will be:

1. We will observe for 60 minutes the area within the optimum radius Ψ (given the zenith distance θ of the GRB) in the direction of the GRB before the time when the GRB is occuring. This way we could estimate the background rate μ_b at that time.

2. The upper limit of signal event rate μ_s will be determined by calculating the upper limit of the Feldman-Cousins confidence interval, given the estimated number of background μ_b, the number of observed events n_{obs} and the required confidence limit $\alpha = 90\%$.

3. The compatibility of the observed events with the background-only hypothesis will be calculated by the likelihood ratio method.

The simulation suggests that no event will be observed during the ON period and at most a couple background events during the OFF period. This should also be the case when we unblind the data and look at it, unless there is an enhancement of TeV γ-rays production at the source itself. Such an enhancement could occur when a more efficient channel of TeV γ-ray production takes place in the GRB, for example the decay of secondary pions in the GRB fireball into neutrinos and high-energy γ-rays (Waxman & Bahcall, 1997; Fragile et al., 2004).

Should such enhancement do occur, the number of signal events would increase dramatically and it is not impossible that they are detectable even by ANTARES.

11.7 The result of data unblinding

THE UNBLINDING proposal has been granted on July 25 2012, and the analysis was performed according to the proposal.

The data from run number 41812 were reconstructed with the `aafit v0r9` algorithm. The Julian Date in the data is used to determine the time of arrival relative to T_0 of the GRB, and local coordinates are used to determine the direction.

For GRB 090709A, the beginning of the on-time is taken to be -66.665 s with respect to the trigger time, and the end of it is taken to be 509.035 s after the alert time. Both values as well as the trigger time are taken from Butler, Bloom & Poznanski (2010).

The off-time is defined to be 1 hour before the on-time. Applying the cuts and knowing the local direction of the GRB at the time it happened, no event were observed during the on-time for both the MDP and MRF cuts. During the off-time, one event was observed for the MDP cut, while 2 events for the MRF cut were

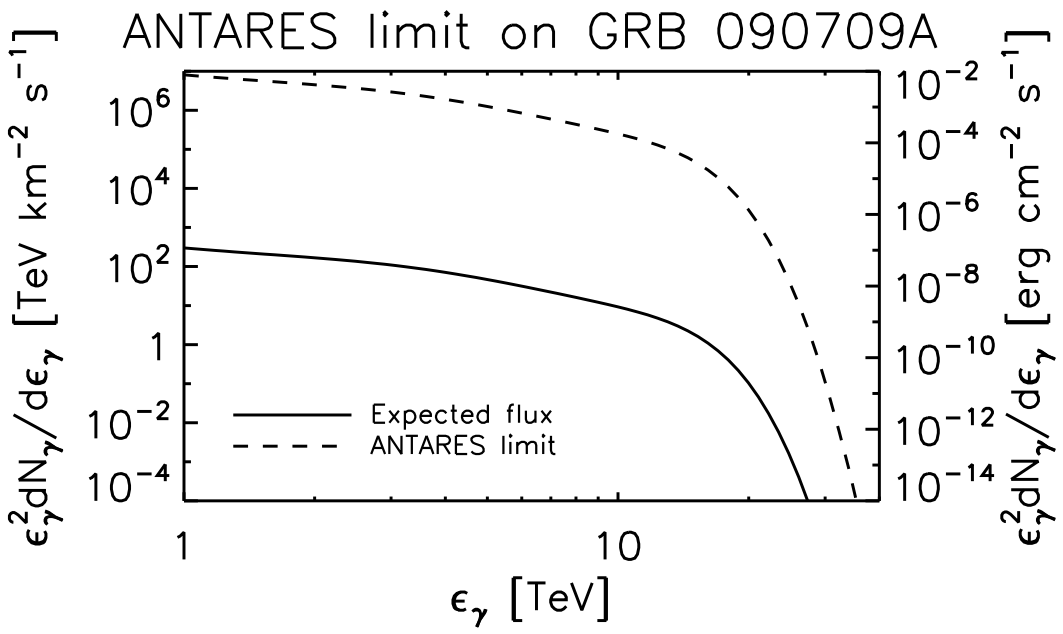

Figure 11.12: The 90% confidence level of the sensitivity of the ANTARES Telescope to GRB 090709A, shown here in dotted lines. The theoretical photon spectrum is shown in solid lines.

observed. The observation of the 2 events after the MRF cuts were administered implies that the number of background is $n_{\text{bg}} = 0.32$ during the on-time.

The sensitivity plot is shown in Figure 11.12. At 10 TeV, the photon is $\phi(10\ \text{TeV}) = 9.25 \times 10^{-2}\ \text{TeV}^{-1}\ \text{km}^{-2}\ \text{s}^{-1}$. By means of Equation 11.17, the ANTARES upper limit is then

$$\phi_{90}(10\ \text{TeV}) = 2.5 \times 10^{3}\ \text{TeV}^{-1}\ \text{km}^{-2}\ \text{s}^{-1}. \tag{11.18}$$

Compared to the expected sensitivity shown in Figure 11.11, the unblinding result is consistent with the expected sensitivity.